A Model of a Tropical Squall Line Boundary Layer Wake

MELVILLE E. NICHOLLS AND RICHARD H. JOHNSON

Department of Atmospheric Science, Colorado State University, Fort Collins, CO 80523

(Manuscript received 14 September 1983, in final form 28 June 1984)

ABSTRACT

A composite analysis has recently been made of the boundary layer associated with the squall line that moved through the GATE ship array on 12 September 1974. That observational study has motivated a modeling investigation of the recovery of the squall boundary layer. The zero-order model of the growth of an unstable boundary layer, as modified by Lilly, and the general structure entrainment model developed by Deardorff are used in order to simulate the wake recovery and to make more explicit the factors influencing the evolution of the mixed layer. A procedure is developed for obtaining the two-dimensional fields of mixed layer depth, specific humidity and dry static energy by formulating the model equations relative to the squall system in natural coordinates.

The results of this study confirm what others have shown, namely, that in the squall wake, mixed layer growth is inhibited mainly by the downward vertical velocity at the top of the mixed layer. Our analysis indicates a large stability above the mixed layer inversion which also plays a significant role in inhibiting growth. The asymmetrical structure of the mixed layer height behind the squall is well simulated, and reasonable agreement is obtained between predicted and observed thermodynamic fields. Large negative gradients of specific humidity atop the inversion appear important in explaining the mixed layer drying for this squall line. Modeling results reveal that precipitation evaporation in the squall wake has a significant effect on the mixed layer height and thermodynamic variables.

1. Introduction

Downdrafts associated with deep convective systems significantly modify the boundary layer,[1] leading to substantially increased fluxes of sensible and latent heat over the tropical oceans. Within the tropical eastern Atlantic region during GATE (GARP Atlantic Tropical Experiment), downdraft-modified boundary layers or "wakes" accompanying precipitation systems were found on the average to cover about 30% of the total area (Gaynor and Mandics, 1978; Gaynor and Ropelewski, 1979). If modeling of these mesoscale systems is to be attempted, the proper treatment of the boundary layer may be an important consideration since it could have a significant effect on the dynamics of these systems. It is also important to understand the effects of deep convective systems on the boundary layer so they might be parameterized in large scale models.

This paper reports on a modeling study of mixed layer recovery following the passage of a squall line that moved through the GATE array on 12 September 1974. Results of the observational study have already been reported by Johnson and Nicholls (1983) (hereafter referred to as JN). Johnson and Nicholls were motivated by the work of Gamache and Houze (1982) who have obtained, by a rawinsonde compositing procedure, a coherent description of the three dimensional structure of this squall line. They selected a 9-hour period during which the radar structure of the squall was approximately in steady state and composited GATE ship array soundings relative to the center of the squall radar echo. Likewise we have used the same compositing procedure but confined our investigation to the boundary layer accompanying the squall.

The 12 September squall line seems to be characteristic of a particular type of squall line that is occasionally found off the coast of West Africa at about 15°N, although much more frequently over land. It has been shown by Aspliden *et al.* (1976) and Payne and McGarry (1977) that the development of squall lines over West Africa is related to the passage of large-scale wave disturbances that occur in association with the 700 mb east African jet. The preferred location for squall development is in advance (¼ to ⅛ of a wavelength ahead) of the wave trough axis at 700 mb between 10° and 15°N. The squall lines that develop move westward at an average speed of 16 m s^{-1} (Payne and McGarry, 1977). They seem to be more intense over land than over the ocean presumably due to stronger surface heating and, in

[1] In this study we regard the boundary layer as consisting of the surface layer, mixed layer and transition layer. The transition layer is the region between the top of the well-mixed layer and the base of nonturbulent stable air above. It can often be identified by a temperature inversion and a rapid decrease in specific humidity occurring through a depth of about 100 m.

fact, often decay rapidly as they move over the cooler sea surface.

Two models have been used in this study to explore the factors controlling mixed layer development following the passage of the squall line: a zero-order jump model in which there are discontinuities in the thermodynamic fields at the top of the mixed layer (e.g., Lilly, 1968), and the general structure entrainment model (hereafter referred to as the GSEM; Deardorff, 1979), which more realistically includes a finite depth transition layer. Previous modeling studies of mixed layer recovery following the passage of a squall have been made by Zipser (1977) and Fitzjarrald and Garstang (1981b), using the zero-order jump model. Zipser's results showed that mesoscale sinking behind the squall line could account for the shallow mixed layers. He hypothesized that the delayed minimum in specific humidity that occurs in the squall wake (unlike the temperature, which reaches a minimum in the heavy rainfall or convective region) to be due to a large entrainment rate of dry air from above the mixed layer associated with subsidence. Fitzjarrald and Garstang (1981b) discussed in detail some of the major factors controlling boundary-layer wake recovery and obtained fairly good agreement with observations of mixed layer height, temperature and humidity for the 12 September squall line. They suggested the entrainment rate and hence drying was also large because of rapid mixed layer growth. The composite analysis presented in JN enables a simulation of the two dimensional fields of mixed layer height, specific humidity and dry static energy to be carried out for the whole of the wake region. Advective and diabatic effects are included as well as the time varying fields of surface fluxes and lapse rates. We obtain reasonable agreement with observations, as do Fitzjarrald and Garstang, but for significantly different values of some of the externally specified parameters. In this paper we attempt to clarify the magnitude and combined effect of the factors controlling boundary layer wake recovery for the 12 September squall line.

2. Composite squall line fields

During the period of our composite analysis (0900–1800 GMT 12 September 1974), soundings at 3-hour intervals were obtained from most of the 15 GATE A/B scale array ships. Hourly positions of the leading edge of the squall radar echo (taken from the paper of Gamache and Houze, 1982) are shown in Fig. 1 for the period 0900 to 2100 GMT. During this time the squall line moved southwestward across the region at an average speed of 13.5 m s^{-1}. Estimated center positions of the squall line at each hour are indicated by crosses. The reader is referred to Gamache and Houze (1982) for details regarding the composite analysis and compositing procedures. A composite

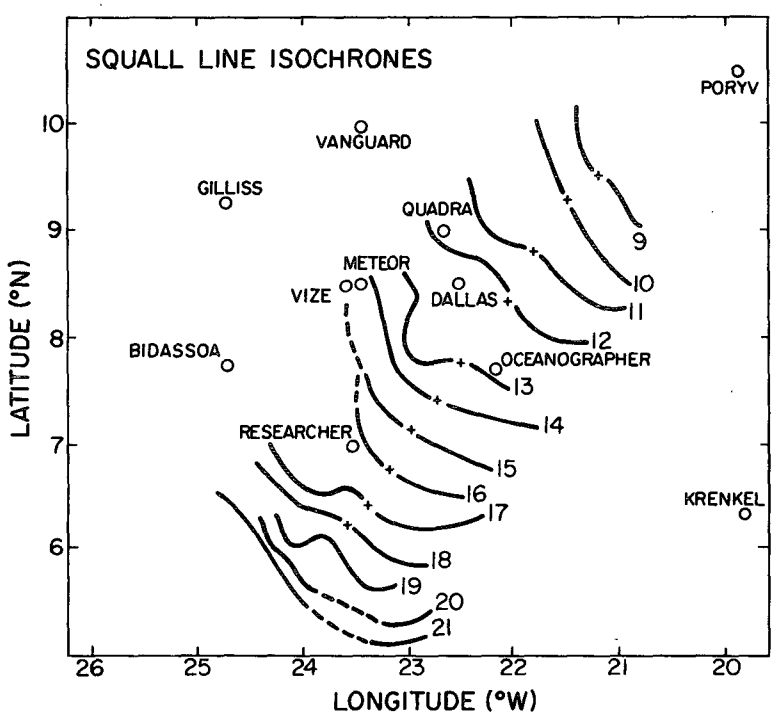

FIG. 1. Isochrone analysis of leading edge of squall line for the period 0900–2100 GMT 12 September 1974 (redrafted from Gamache and Houze, 1982). Crosses mark the center position of the squall. Ship positions are indicated.

analysis of the boundary layer for this squall line has been presented in JN. Additional composite fields required for this modeling study are rainfall rate, surface buoyancy flux, vertical velocity and gradient of specific humidity atop the mixed layer inversion.

Two components of the squall radar echo have been identified by Gamache and Houze using ship-based weather radars: 1) the squall line itself and 2) the post-squall anvil region. The former feature refers to the cumulonimbus convection on the leading edge of the squall system. The post-squall anvil region refers to the nearly continuous stratiform cloud system of mesoscale (~200 km) dimension trailing the squall line (Houze, 1977; Zipser, 1977). The average boundaries of these squall components will be outlined in subsequent figures.

Figure 2 shows the rainfall rates from the anvil as composited by Gamache and Houze (1983). They obtained an average rainfall rate of 2.7 mm h^{-1} over the whole anvil although in some regions it can be seen to be significantly larger. The surface buoyancy flux formulated in terms of the virtual static energy is given by (e.g., Arakawa and Schubert, 1974)

$$F_{s_{v_0}} = S_0 + 0.61 c_p T E_0,$$

where S_0 and E_0 are the sensible heat and moisture fluxes, respectively and T a reference temperature. The surface virtual static energy flux within the squall wake is shown in Fig. 3. It is primarily the surface cooling by convective downdrafts that contributes to enhanced virtual static energy flux over most of the anvil region (JN). Maximum values of virtual static energy fluxes occur on the southeast side of the squall system and a relative minimum occurs near the center of maximum surface divergence where winds are very light (JN).

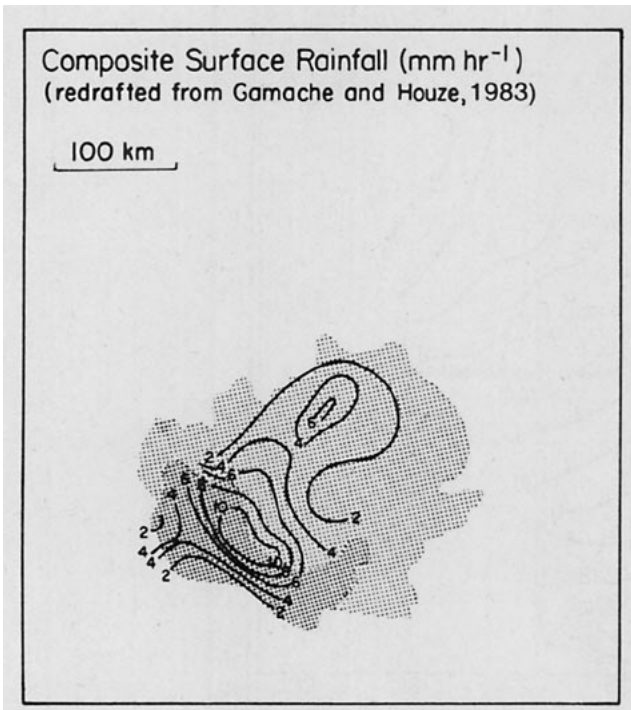

FIG. 2. Composite surface rainfall (mm h^{-1}) (redrafted from Gamache and Houze, 1983). Dark and light shaded regions denote squall line (convective echo) and anvil (stratiform echo) regions, respectively.

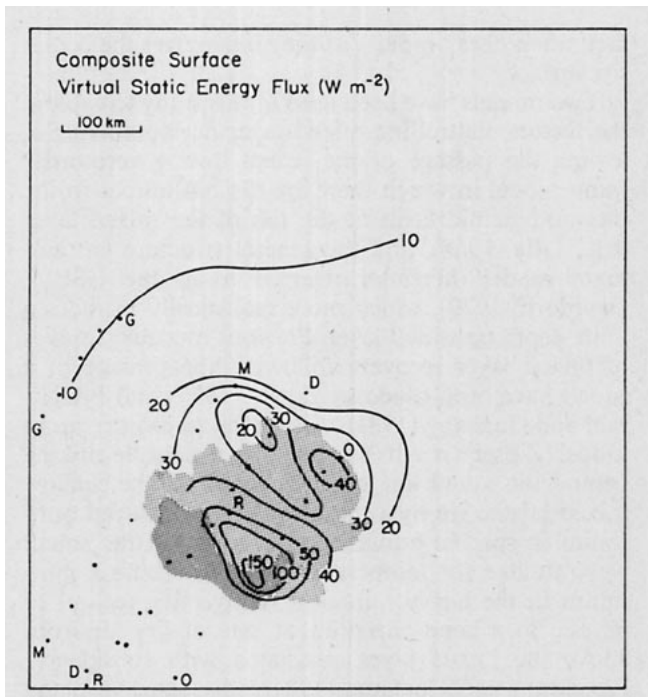

FIG. 3. Composite surface virtual static energy flux (W m^{-2}). Hourly positions of *Gillis* (G), *Meteor* (M), *Dallas* (D), *Researcher* (R), and *Oceanographer* (O) are indicated by dots.

a. *Vertical velocity field*

The vertical velocity at the top of the mixed layer has an important influence on its growth. Horizontal wind velocities measured by rawinsonde are, in some instances, of limited accuracy very close to the sea surface (as discussed in JN). We have chosen to determine the vertical velocity at 970 mb using the divergence fields at this level and at the surface, as a reasonable compromise between being low enough to be close to the mixed layer height and having fairly accurate wind data. The vertical velocity at the top of the mixed layer is then obtained by interpolating between the surface and 970 mb (or extrapolating if above 970 mb). The vertical velocity field at 970 mb has been determined from the continuity equation in p-coordinates:

$$\omega\,(970\text{ mb}) = \omega_{\text{sfc}} - \int_{P_{\text{sfc}}}^{970\text{ mb}} \nabla_H \cdot \mathbf{v}\,dp \approx \langle \nabla_H \cdot \mathbf{v} \rangle \Delta p, \tag{1}$$

where the angle brackets refer to the average between

p_{sfc} and 970 mb. It can be shown from the composite analysis of the pressure field in JN that it is a good approximation to let $\omega_{sfc} \equiv 0$. Wind vectors have been plotted at the surface and at 970 mb and a subjective streamline and isotach analysis has been carried out. Divergences were calculated at these levels using a 60 km grid, and then averaged so as to obtain ω (970 mb).

We use the following interpolation formula for the vertical velocity,

$$w(z) = \frac{w\,(375\text{ m})}{0.6}\,(1 - e^{-z/409}, \qquad (2)$$

where z = height in m.

This gives a similar profile to that found by Gamache and Houze (1982) for the anvil downdraft below 1 km (see their Fig. 13). Below 1 km their divergence profile, which is an average over the anvil region (see their Fig. 12), shows a fairly linear decrease with height. If the gradient of divergence with height is approximately constant, then our method of computing the mean divergence by taking the average between two levels is reasonably good. However, in regions where divergence does not decrease linearly with height, for instance beneath the 970 mb diffluence center where it actually increases with height (JN), some error in the downward vertical velocity at the top of the mixed layer (up to 20% too large) is incurred using Eq. (2).

The surface and 970 mb flow fields which are used to compute divergences differ slightly from JN since some attention there was given to soundings at 2100 GMT in regions of sparse data, although the squall system was only reasonably approximated by steady state between 0900–1800 GMT. The 2100 GMT soundings are felt to be too late for use in the composite and have been neglected. The vertical velocity field at 970 mb (375 m) is shown in Fig. 4. It shows a region of strong mesoscale subsidence behind the squall line, offset somewhat from the surface diffluence center (see JN, Fig. 5) due to the increase in wind speed that occurs towards the squall front. Well behind the squall line weak upward vertical motion is diagnosed.

b. Gradient of specific humidity above the transition layer

Above the mixed-layer top a transition layer, about 100 m thick, exists which normally has a very stable lapse rate of dry static energy (Fitzjarrald and Garstang, 1981a). The growth and thermodynamic structure of an entraining mixed layer is dependent on the gradients of dry static energy and specific humidity above the transition layer. The composite analysis of the gradient of dry static energy has been presented in JN and shows a significant increase in the stability of the air above the transition layer in the wake of the squall line. Before presenting the composite analysis of the gradient of specific humidity, it is helpful to try and understand the development of the thermodynamic profiles in order to obtain a clearer physical picture of the mixed layer recovery process. Further, this understanding will be useful in guiding the analysis itself.

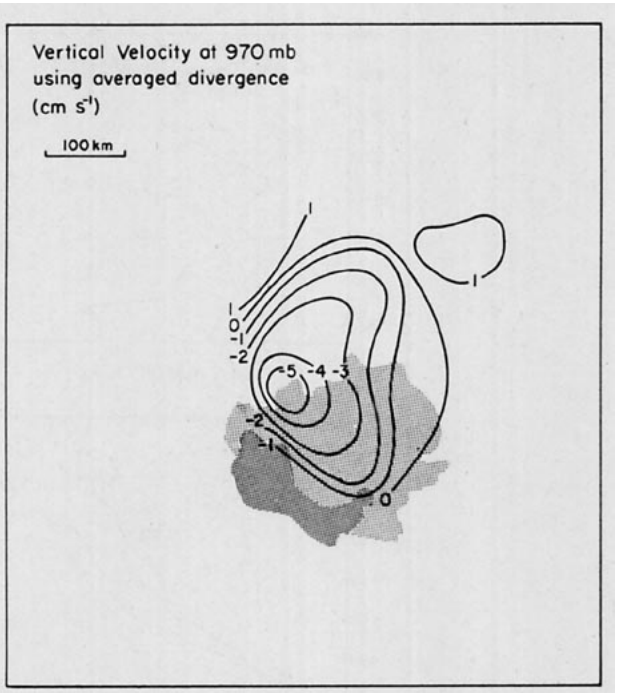

FIG. 4. Vertical velocity field (cm s^{-1}) at 970 mb within the squall wake.

In Fig. 5 profiles of dry static energy and specific humidity occurring in the wake of the squall line are shown. The ships *Oceanographer, Researcher, Dallas* and *Meteor* are denoted by O, R, D and M, respectively, and the time of the sounding (GMT) is given in parenthesis. Figure 5a shows soundings taken fairly close to the squall front (~50–150 km behind convective echo region) and Fig. 5b soundings further behind (>150 km). A consistent pattern in specific humidity can be seen with relative maxima occurring ~600–1000 m above the sea surface. In most cases a mixed layer can be observed, above which a sharp gradient identifies the transition layer (this can usually be seen in both the q and s profiles). The gradient of specific humidity above the transition layer is seen to be highly variable taking both positive and negative values. The O(1513) sounding which was taken just behind the convective echo region shows no evidence of a mixed layer in either the specific humidity or dry static energy profiles. Figure 6 shows moist static energy ($h = c_pT + g\dot{z} + Lq$) profiles for three soundings ahead of the squall line and three soundings within the squall wake. There is a considerable decrease in the low level moist static energy after the passage of the squall line. Also noticeable in the soundings within the squall wake, in particular for

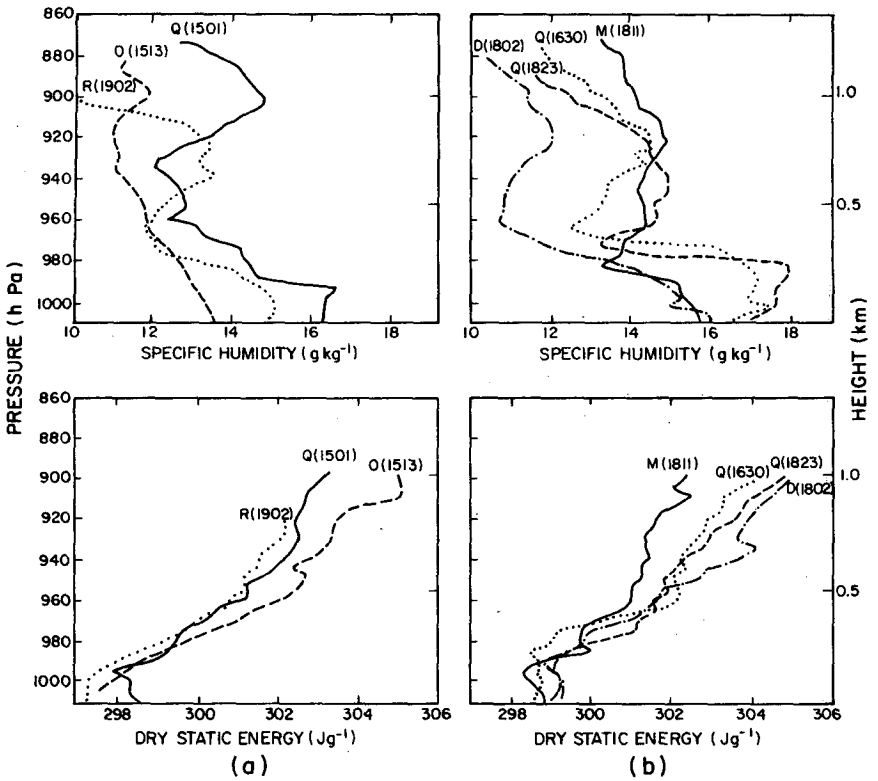

FIG. 5. Profiles of specific humidity and dry static energy within the squall wake: (a) Soundings taken fairly close to the squall front (~50–150 km behind convective echo region) and (b) sounding further behind (>150 km).

R(1902) and Q(1501), are relative maxima in moist static energy occurring above the surface.

The following hypothetical model is suggested to explain these observations. Convective downdrafts occur in cores or cells and result in air originally at about 3 km being brought down to the surface (Betts, 1976). Idealized schematic profiles of the modification of the dry static energy and specific humidity from ambient values ahead of the squall line to values just behind the region of strong convective downdrafts are shown in Figs. 7a, b. The dry static energy and specific humidity profiles in 7b should be compared with the O(1513) sounding (Fig. 5). Just after the squall passage the mixed layer is absent or extremely small. The formation of the relative maximum in specific humidity at 1 km or higher from the surface is hypothesized to occur due to dry air (in the sense that q is less) from the convective downdrafts (the replacement of low level air ahead of a squall line by drier air from convective scale downdrafts is discussed by Barnes and Garstang, 1982) spreading out beneath moister air. This moister air overlying the downdraft outflow could have originated ahead of the squall line and flowed around the intense but relatively isolated convective cells. Alternatively, Gamache and Houze's, 1982, Fig. 7b, 850 mb relative wind field shows flow entering the squall system from the east over much of the anvil region, without passing through the squall front. The profiles of moist static energy within the squall wake shown in Fig. 6 are consistent with the idea that air from convective downdraft cores spreads out at the surface beneath air which has not originated from such a high level. The depth of this convective outflow seems to be about 1 km at 100 km behind the squall front and decreases within the mesoscale subsidence region. The low moist static energy of the air above the relative maximum compared with that of the air preceeding the squall line (see Fig. 6) may be due to mesoscale subsidence. Hence, although Fig. 6 suggests that the depth of the modified profile (i.e., the region having a lower moist static energy than the air ahead of the squall line) is greater than 1.5 km, the depth of the air actually originating from convective downdraft cores is probably less than this. The O(1513) sounding taken just behind the convective echo region shows an almost constant moist static energy profile below 920 mb all the way down to the surface. The relative surface maximum occurring in the R(1902) and Q(1501) profiles can be attributed to sensible and latent heat exchanges at the sea-air interface associated with mixed layer recovery.

To understand how the profile in Fig. 7b might develop as we follow the air parcel trajectory, it helps

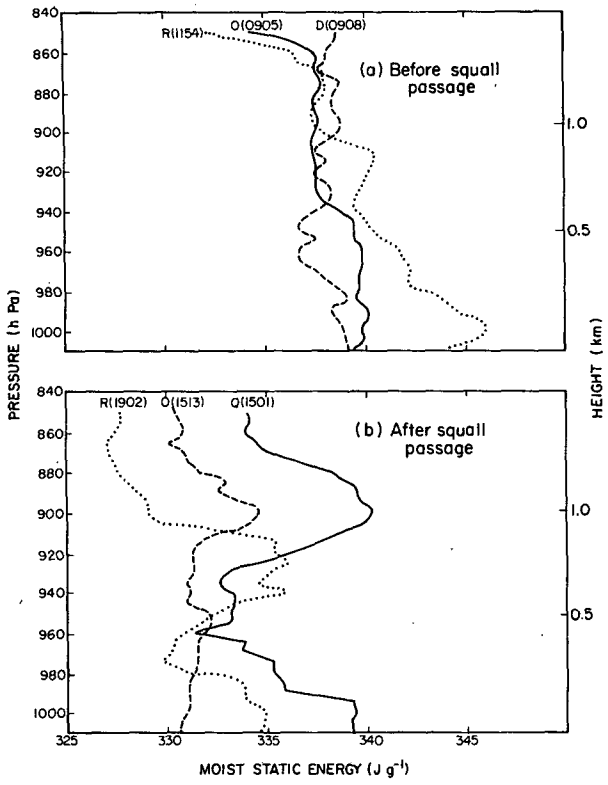

FIG. 6. Moist static energy profiles for (a) three soundings ahead of the squall line and (b) three soundings within the squall wake.

to consider the equations for the rate of change of the gradients of virtual static energy and specific humidity following the motion in the stable air above the transition layer. (Similar equations were used by Carson, 1973.) For the case of constant divergence (with height) and no moisture or diabatic heating sources

$$\frac{d_H\Gamma_s}{dt} = -\Gamma_s \frac{w(z)}{z}, \tag{3}$$

$$\frac{d_H\Gamma_q}{dt} = -\Gamma_q \frac{w(z)}{z}, \tag{4}$$

where Γ_s ($=ds/dz$) is the gradient of dry static energy, Γ_q ($=dq/dz$) is the gradient of specific humidity (note that gradients are the negative of the lapse rates) and $d_H/dt = \partial/\partial t + u\partial/\partial x + v\partial/\partial y$. These equations indicate that subsidence will act to increase the magnitude of the gradient, and further, that this increase is proportional to the gradient itself. If we were to follow, over a 50–100 km distance, the trajectory relative to the squall line of a column of air with profiles like that in Fig. 7b, we might qualitatively expect the new profiles to look like those in Fig. 7c. Subsidence has brought the relative maximum in the specific humidity profile closer to the surface and the mixed layer has started to recover. Furthermore, the mixed layer is growing into a region having a strong negative gradient of specific humidity. The gradient of dry static energy above the transition layer is also increasing as long as subsidence is occurring (at least as long as Γ_s is fairly constant with height). Compare the profiles in Fig. 7c to those of *Researcher* (1902) and *Quadra* (1501) in Fig. 5. As subsidence continues, the mixed layer eventually grows into air where the gradient of specific humidity changes sign and becomes positive, as shown in Fig. 7d [cf. soundings of *Meteor* (1811) and *Quadra* (1823) in Fig. 5].

In Fig. 8 the composite analysis of the gradient of specific humidity (dq/dz) above the transition layer is shown. A region of large negative gradients is evident in the middle of the squall wake (based on our subjective analysis) with positive gradients to the rear. Strong gradients (10 g kg^{-1} km^{-1} or greater in magnitude) only exist through a depth of about 100–200 m above the transition layer. We have estimated the gradient of specific humidity above the transition layer for R(1902) to be -10 g kg^{-1} km^{-1} (see Fig. 5). Since no well defined transition layer can be identified there is considerable uncertainty in this estimate. The asterisks denote the soundings of *Dallas* (1802) and *Quadra* (1630) (see Fig. 5) which are difficult to classify and could have either negative or positive gradients of specific humidity above the mixed layer.

3. Models for wake recovery

a. Zero-order jump model

A version of the zero order jump model developed by Ball (1960) and Lilly (1968) is used that 1) includes the effects of advection, variable lapse rate of both virtual static energy and specific humidity and the vertical velocity at the top of the mixed layer; 2) uses the diagnosed buoyancy and latent heat fluxes; and 3) allows inclusion of radiative and evaporative cooling.

The Monin-Obukhov length in the wake is fairly small (~25 m), indicating that buoyancy-driven turbulence dominates in the mixed layer and the simple models referred to above can be applied to this situation. Another important consideration is the production of turbulence due to wind shear in the transition layer. Deardorff (1979) estimated using results from the study by Moore and Long (1971) that the shear-driven entrainment becomes of equal or greater importance than convectively driven entrainment when $\Delta\bar{u} > 6w_*$ where $\Delta\bar{u}$ is the magnitude of the mean flow difference across the interfacial layer, and w_* the convective scale velocity given by

$$w_* = [(g/s_v)h(\overline{w's_v'})_0]^{1/3}, \tag{5}$$

where h is the mixed layer depth and $(\overline{w's_v'})_0$ is the vertical flux of virtual static energy at the sea surface. If the transition layer depth is about 100 m and if we estimate $\Delta\bar{u}$ from wind profiles (not shown), the ratio of $\Delta\bar{u}$ to $6w_*$ takes values between $\frac{1}{12}$–$\frac{4}{5}$ with

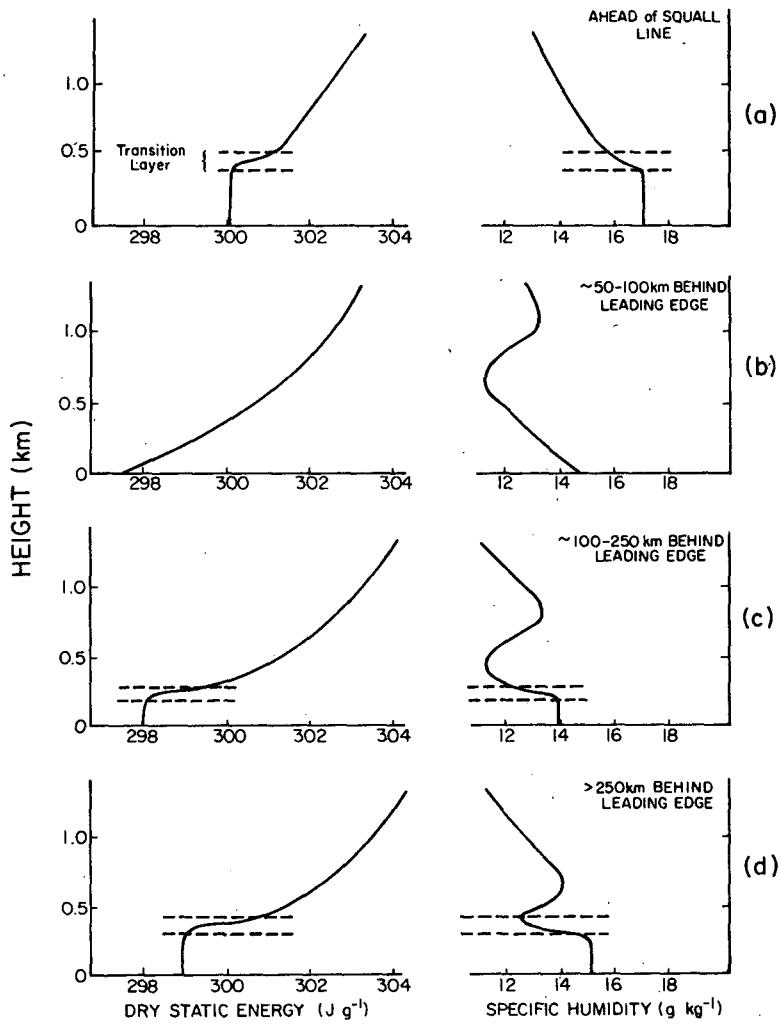

FIG. 7. Idealized schematic profiles showing the modification of dry static energy and specific humidity that occurs with the passage of the squall system. Thermodynamic structure of air (a) ahead of squall line, (b) just outside the region of convective scale downdrafts (~50–100 km behind leading edge of squall line), (c) middle of squall wake (~100–250 km behind leading edge), (d) rear of squall wake (>250 km behind leading edge).

a mean of $\sim\frac{1}{2}$ within the squall wake. The high value of this ratio for some soundings indicates that turbulent production due to wind shear could be significant. It should be pointed out that unlike the thermodynamic variables momentum did not appear to be well mixed within the mixed layer and no distinct jump in wind speed $\Delta\bar{u}$ was observed across the transition layer. However, the limited accuracy and vertical resolution of the low level wind measured by rawinsonde (as noted in JN) may preclude the drawing of definitive conclusions about the mixed layer wind structure.

The zero-order model is highly idealized and considers zero-order discontinuities or jumps in virtual static energy and specific humidity (Δs_v and Δq) at the top of the mixed layer. The equations for the growth of the mixed layer height and inversion strength are obtained in the following manner. Reynolds averaging the thermodynamic equation and making the Boussinesq approximation we obtain

$$\frac{\partial \bar{s}_v}{\partial t} + \overline{\nabla \cdot \mathbf{v} s_v} + \frac{\partial}{\partial z}\bar{w}\bar{s}_v + \frac{\partial}{\partial z}\overline{w's'_v} = Q, \qquad (6)$$

where $\mathbf{v}$ is the horizontal velocity and Q represents diabatic effects due to radiation and precipitation evaporation. According to Holle *et al.* (1977), there was considerable low cloudiness behind the squall line; however, the precise heights of these clouds are not well known. Lifting condensation levels for soundings within the squall wake exceed the mixed layer depth by about 200–300 m, so it seems reason-

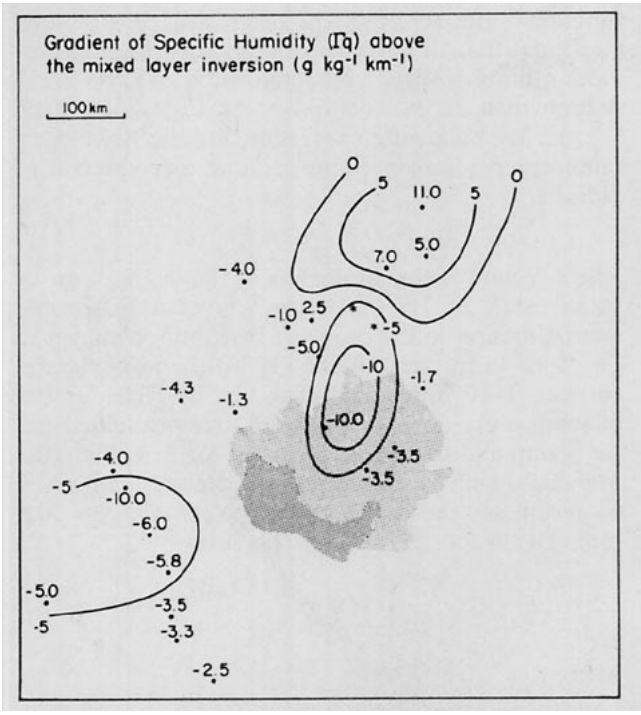

FIG. 8. Composite gradient of specific humidity atop the mixed layer inversion. Asterisks denote soundings for which the sign of the gradient is difficult to determine.

able to assume that the low clouds were above the mixed layer. The low cloud may be associated with the relative maximum in specific humidity occurring above the surface shown in Fig. 5 although saturation is not indicated for these soundings. Based on this information we neglect cloud condensation processes within the mixed layer and transition layer.

We consider infinitesimal distances above and below h to the heights h_+ and h_- respectively, then integrate between these levels. Using Leibniz' rule, taking the limit as $h_+ - h_- \to 0$, and assuming horizontal velocity independent of height, we obtain

$$\frac{\partial h}{\partial t} + \mathbf{v}\cdot\nabla h = \bar{w}_h - \frac{F_{svh}}{\Delta s_v} + \frac{\Delta F_Q}{\rho \Delta s_v}, \tag{7}$$

where $\bar{w}_h$ is the mean vertical velocity at h, F_{svh} the buoyancy flux, and ΔF_Q is the jump in the diabatic heat flux (W m^{-2}) at h. At h_+ we have

$$\frac{d\bar{s}_{vh+}}{dt} = \Gamma_{s_v}\frac{dh_+}{dt} + Q_{h+}, \tag{8}$$

where $\Gamma_{s_v} = \partial s_{vh+}/\partial z$ the gradient of s_v above the discontinuity. Therefore

$$\frac{\partial \Delta s_v}{\partial t} = \Gamma_{s_v}\left(\frac{dh_+}{dt} - \bar{w}_{h+}\right) - (\bar{\mathbf{v}}\cdot\nabla\bar{s}_v)_{h+} - \frac{\partial \bar{s}_{vh-}}{\partial t} + Q_{h+}. \tag{9}$$

Integrating (6) from the surface to h_- we obtain

$$\frac{\partial \bar{s}_{vh-}}{\partial t} + \bar{\mathbf{v}}\cdot\nabla\bar{s}_{vh-} = \frac{F_{sv0} - F_{svh-}}{h_-} + Q_m, \tag{10}$$

where Q_m is the mean diabatic heating term, averaged through the depth of the mixed layer. Substituting (10) into (9), taking the limit as $h_+ - h_- \to 0$ and substituting from (7), we find

$$\frac{\partial \Delta s_v}{\partial t} + \bar{\mathbf{v}}\cdot\nabla\Delta s_v = -\Gamma_{s_v}\left(\frac{F_{svh}}{\Delta s_v} - \frac{\Delta F_Q}{\rho \Delta s_v}\right) + \frac{F_{svh} - F_{sv0}}{h} + \Delta Q, \tag{11}$$

where $\Delta Q = Q_{h+} - Q_m$. The system of equations (7) and (11) is incomplete since the buoyancy flux F_{svh} has not been specified. The conventional closure assumption (Betts, 1973; Tennekes, 1973) is to make it proportional to the surface buoyancy flux, i.e.,

$$F_{svh} = -kF_{sv0}, \tag{12}$$

where k is an entrainment parameter normally considered to have a value between 0.2 and 0.5. Driedonks (1982) recommends a low value for k of 0.2, whereas we have used the slightly higher value 0.25 in this study following Fitzjarrald and Garstang (1981b). Sensitivity to the choice of k is not great as will be discussed later.

Similar equations hold for the specific humidity as for the virtual static energy except the closure assumption is no longer valid. For specific humidity we have

$$\frac{\partial \bar{q}_m}{\partial t} + \bar{\mathbf{v}}\cdot\nabla\bar{q}_m = \frac{F_{q0} - F_{qh}}{h} + E_m, \tag{13}$$

$$F_{qh} = -\Delta q\left(\frac{dh}{dt} - \bar{w}_h\right) + \frac{\Delta F_E}{\rho}, \tag{14}$$

$$\frac{\partial \Delta q}{\partial t} + \bar{\mathbf{v}}\cdot\nabla\Delta q = -\Gamma_q\left(\frac{F_{qh}}{\Delta q} - \frac{\Delta F_E}{\rho \Delta q}\right) + \frac{F_{qh} - F_{q0}}{h} + \Delta E, \tag{15}$$

where $\bar{q}_m$ is the specific humidity in the mixed layer, F_{q0} and F_{qh} the fluxes of specific humidity at the surface and at the top of the mixed layer, respectively, Γ_q the gradient of $\bar{q}$, Δq the jump at h, E_m the mean evaporation rate of precipitation in the mixed layer, $\Delta E = E_{h+} - E_m$, and ΔF_E the jump of the precipitation flux across the transition layer. Substituting (7) into (14) we find

$$-\frac{F_{qh}}{\Delta q} + \frac{\Delta F_E}{\rho \Delta q} = -\frac{F_{svh}}{\Delta s_v} + \frac{\Delta F_Q}{\rho \Delta s_v}. \tag{16}$$

A useful variable, to be referred to later, is the entrainment rate defined by

$$W_{en} = \frac{dh}{dt} - \bar{w}_h. \tag{17}$$

Fitzjarrald and Garstang (1981b) found that the ratio,

$$R = \frac{F_{qh}}{F_{q0}}, \tag{18}$$

is not constant in contrast to the ratio of the fluxes of virtual static energy. We can see from Eq. (13) that mixed-layer drying requires F_{qh} to exceed F_{q0} ($R > 1$).

This model has a discontinuity in the thermodynamic variables at the top of the mixed layer, so that the transition layer is infinitesimal. In reality the transition layer has a finite depth of about 100 m. The height h when applied to the real atmosphere is regarded here as the distance from the surface to the middle of the transition layer rather than the top of the mixed layer. When the mixed layer height is large this distinction probably is not very important; however, since in the squall wake the transition layer is almost as thick as the mixed layer in some regions, it could be significant. This consideration has been the main motivation for also using Deardorff's (1979) General Structure Entrainment Model (GSEM) which allows for a realistic transition layer of finite depth.

b. *Deardorff's general structure entrainment model (GSEM)*

In the GSEM the transition layer depth is a dependent variable and requires a rate equation for its determination. Use of the rate equation suggested by Deardorff (1979, Eq. 46) was found to lead to extremely small transition layer depths of about 20–30 m. This was due to the term representing the effect of the difference in vertical velocity at the top and bottom of the transition layer on its development. If this term is neglected transition layer depths of about 100 m are obtained. Mixed layer height was found to be relatively insensitive to the transition layer depth. Because of the uncertainty with the rate equation, results will be presented here for a fixed transition layer depth of 80 m. Similar to the zero-order model, the GSEM has prediction equations for $\bar{s}_{vm}$, Δs_v, $\bar{q}_m$, Δq and the mixed layer height, which are presented in the Appendix. We refer the reader to Deardorff (1979) for a description of this model.

c. *Treatment of evaporation and diabatic heating*

Evaporation of precipitation falling from the squall anvil is a source of moisture and diabatic heating. Precipitation evaporation rate E is estimated using basically the same development presented by Tripoli and Cotton (1980); however, here we use a Gamma drop size distribution instead of a Marshall-Palmer distribution. Willis (1984) in a detailed study of functional fits to observed drop size distributions concludes that an analytical gamma distribution provides a more realistic characterization of drop evaporation than an exponential one (Marshall-Palmer). We use the following expression for the number of raindrops per unit volume per unit size interval of radius r,

$$N(r) = N_0 r^2 e^{-\lambda r}, \tag{19}$$

where N_0 and λ are parameters of the distribution. A value for λ of 7.5×10^3 m^{-1} gives a reasonable approximation to the drop size distribution shown in Fig. 7 of Leary and Houze (1979) for rainfall rates between 1–10 mm h^{-1} during GATE. The number of small drops ($r < 0.2$ mm) are underestimated but the gamma distribution is more realistic than the Marshall-Palmer distribution which significantly overestimates the number of droplets with $r < 0.5$ mm. The evaporation rate is given by

$$E = G s_l r_r \frac{\lambda^2}{\rho_w}\left[0.15 + \frac{0.18}{\lambda^{3/4}}\frac{(\rho_0 \rho_w g)^{1/4}}{\mu^{1/2}}\right], \tag{20}$$

where

$$G(T, P) = \left[\frac{m_w L^2}{k R_* T^2} + \frac{R_* T}{e_s(T) D m_w}\right]^{-1}, \tag{21}$$

k molecular diffusivity of heat,
D molecular diffusivity of water vapor,
m_w molecular weight of water,
ρ_0 density of air,
ρ_w density of water,
e_s saturated vapor pressure,
r_v water vapor mixing ratio,
r_{vs} saturated water vapor mixing ratio,
s_l subsaturation ($1 - r_v/r_{vs}$),
r_r mixing ratio of rain, and
μ dynamic viscosity.

Other symbols have their usual meaning. The variables which need to be specified are the rainfall rate, the water vapor mixing ratio and the temperature.

The diabatic heating written in flux form is

$$Q = -\frac{1}{\rho}\frac{\partial F_Q}{\partial z} = -\frac{1}{\rho}\frac{\partial F_R}{\partial z} + \frac{L}{\rho}\frac{\partial F_E}{\partial z}, \tag{22}$$

where F_R is the radiation flux and F_E the precipitation flux (we assume no storage of liquid water). Hence, we have divided the diabatic heating into two parts, that due to radiation and that due to precipitation evaporation. Diabatic heating due to radiation is complicated by the presence of the squall anvil. In clear skies in the GATE mixed layer, it is probably about -2°C day^{-1} (Cox and Griffith, 1979).

If we consider the jump in the diabatic heating flux ΔF_Q across the transition layer, we have

$$-\Delta F_Q = -\Delta F_R + L \Delta F_E, \tag{23}$$

where

$$\Delta F_E = -\int_h^{h_t} \rho E(z)dz \approx -\rho E_{mt}\Delta h, \qquad (24)$$

h and h_t refer to the top of the mixed layer and transition layer respectively, and E_{mt} is the mean evaporation rate in the transition layer. Hence Eqs. (20) and (24) can be used to determine E_m, ΔE, ΔF_E and the associated diabatic heating due to precipitation evaporation if the rainfall rates and thermodynamic profiles beneath the squall anvil are known. A difficulty arises if this method is used to estimate the flux terms ΔF_Q and ΔF_E for the zero-order model. If we choose a finite Δh in order to estimate ΔF_Q, which appears in the growth rate equation (7), this term will always be nonzero if rainfall is occurring. This means that if diabatic heating due to evaporation were constant throughout the mixed layer depth and the inversion this term would effect the mixed layer growth rate. However, physically the effect on the growth rate must arise from a difference in the heating rates of the mixed layer and inversion. For the GSEM, Eq. (A1) for the entrainment rate shows that in the case of constant heating the two terms $-\alpha(F_{Qh_1} - F_{Q0}) + (F_{Qh_2} - F_{Qh_1})$ cancel exactly (where $F_{Qh_1} - F_{Q0}$ and $F_{Qh_2} - F_{Qh_1}$ are the flux differences across the mixed layer and transition layer, respectively). For this reason results for diabatic heating will be presented for the GSEM, although for the particular case studied here using the above method to determine ΔF_Q and ΔF_E for the zero order model gave similar results.

d. *Numerical procedure*

Both models have prediction equations for h, $\bar{s}_{vm}$, Δs_v, $\bar{q}_m$ and Δq. In the case of the zero-order model these are (7), (10), (11), (13) and (15), respectively. These equations can be solved once we have specified from observations the initial values of the quantities and the fields of $\mathbf{v}$, $\bar{w}_h$, F_{sv0}, Γ_{s_v}, F_{q0} and Γ_q.

The method used to solve these equations is similar to that used by Schubert *et al.* (1979a,b), in that the equations are formulated in the natural coordinate system. However, we also transfer to a coordinate system moving with the squall line which is assumed to be in the steady state and moving at 13.5 m s^{-1} in a fixed direction. Relative to the squall line the air in the mixed layer moves towards the rear of the system (except perhaps right at the gust front). To determine the relative streamlines and isotachs the mean velocity in the mixed layer was estimated by averaging the wind speed between the surface and the top of the mixed layer. The velocity at the top of the mixed layer was estimated by linearly interpolating (or extrapolating) between the surface and 970 mb using the composite analyses of the wind fields at these levels and of the mixed layer height. The average velocity of the squall line was then subtracted from the mean velocity field of the mixed layer to obtain the relative streamlines and isotachs shown in Fig. 9. (These are mean mixed-layer streamlines). The procedure is then to numerically integrate the equations along each streamline once initial values of the variables have been specified.

For the zero-order model the equations in natural coordinates relative to the squall line are

$$v_r \frac{\partial h}{\partial l} = \bar{w}_h - \frac{F_{svh}}{\Delta s_v} + \frac{\Delta F_Q}{\rho \Delta s_v}, \qquad (25)$$

$$v_r \frac{\partial \bar{s}_{vm}}{\partial l} = \frac{F_{sv0} - F_{svh}}{h} + Q_m, \qquad (26)$$

$$v_r \frac{\partial \Delta s_v}{\partial l} = -\Gamma_{s_v}\left(\frac{F_{svh}}{\Delta s_v} - \frac{\Delta F_Q}{\rho \Delta s_v}\right) + \frac{F_{svh} - F_{sv0}}{h} + \Delta Q, \qquad (27)$$

$$v_r \frac{\partial \bar{q}_m}{\partial l} = \frac{F_{q0} - F_{qh}}{h} + E_m, \qquad (28)$$

$$v_r \frac{\partial \Delta q}{\partial l} = -\Gamma_q\left(\frac{F_{qh}}{\Delta q} - \frac{\Delta F_E}{\rho \Delta q}\right) + \frac{F_{qh} - F_{q0}}{h} + \Delta E, \qquad (29)$$

where

$$F_{svh} = -0.25F_{sv0}, \qquad (30)$$

$$F_{qh} = \Delta q\left(\frac{F_{svh}}{\Delta s_v} - \frac{\Delta F_Q}{\rho \Delta s_v} + \frac{\Delta F_E}{\rho \Delta q}\right); \qquad (31)$$

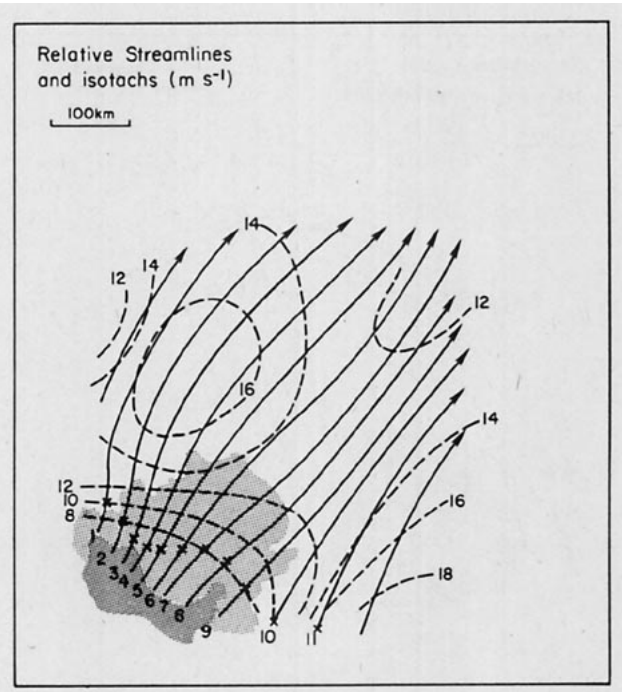

FIG. 9. Relative mixed layer streamlines (solid lines) and isotachs (dashed lines). Each initial position for model integration along eleven streamlines denoted by x.

v_r is the wind speed relative to the squall line and l is the distance along a streamline. The equations for h and Δs_v were solved using the Runge-Kutta fourth-order method. The integrations are performed along the eleven streamlines shown in Fig. 9 with the values of surface fluxes, vertical velocity, horizontal velocity and lapse rates being specified from the observed values at 30 km intervals. The space differencing used was 1 km; a cubic spline routine was used to interpolate between the 30 km increments.

4. Results

a. *Without precipitation evaporation and diabatic heating*

The modeling approach taken here is to specify the surface fluxes from observations allowing no feedback of predicted mixed layer temperature and specific humidities on the fluxes. The reason for not using a fully interactive model in which sea surface fluxes are predicted is that they would depend on composite fields of all the quantities that go into the model (in addition we would need a composite analysis of sea surface temperature) whereas, it seems more reasonable to use shipboard boom data to determine fluxes (JN).

The initial starting points for the model integrations, which lie on the periphery of the area of very stable air in the wake (JN), are shown by the crosses in Fig. 9. The initial values used for the zero-order model were h = 150 m, Δs_v = 0.4 J g^{-1} and Δq = −0.7 g kg^{-1} (the jump in dry static energy for this case is Δs ~ 0.52 J g^{-1}) for streamlines 1–9, $h(10)$ = 230 m and $h(11)$ = 360 m. Initial values of virtual static energy and specific humidity were determined from the composite analyses of these fields. There is some uncertainty in the initial values of Δs_v and Δq that should be used; however, results are not very sensitive to reasonable variations of these quantities (as found by others, e.g., Tennekes, 1973: Johnson, 1981).

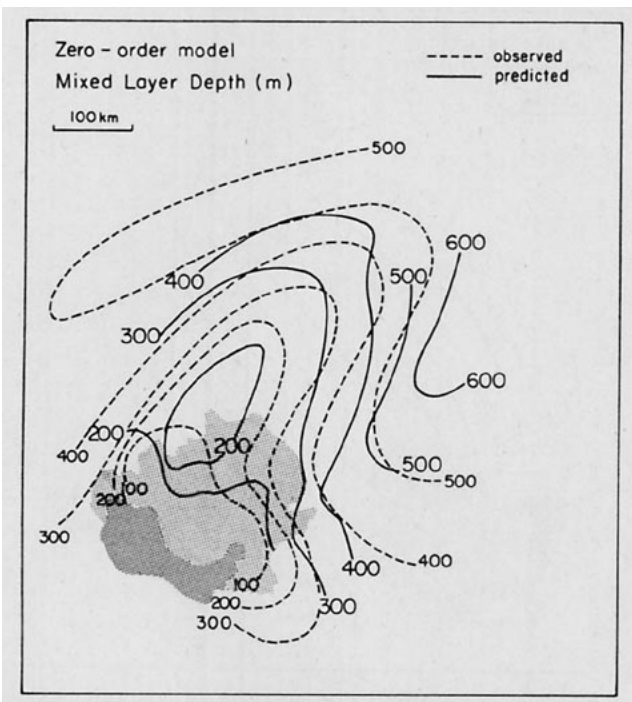

FIG. 10. Mixed layer depth (m) predicted by the zero-order model (solid lines). Dashed lines show observed values.

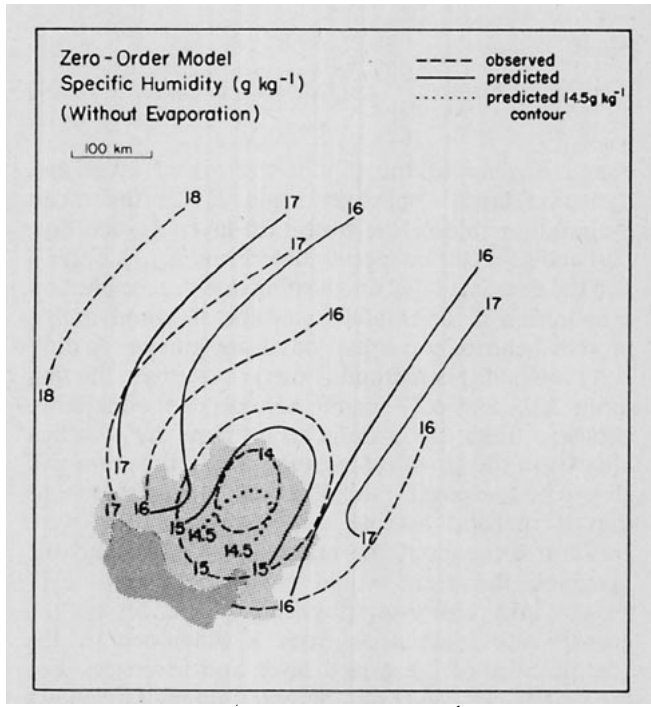

FIG. 11. Mixed layer specific humidity (g kg^{-1}) predicted by the zero-order model without precipitation evaporation and diabatic heating. Dashed lines show observed values.

Figure 10 shows model results for the mixed layer depth using the zero-order jump model. Fairly good agreement is found with the composite analysis although mixed layer recovery is slower than observed on the north side of the wake. This could be partly due to an overestimate of the downward vertical velocity in this region as discussed earlier. (note that the zero-order mixed layer depth should be regarded as the height of the middle of the transition layer, about 50 meters greater than the actual mixed layer depth). Figures 11 and 12 show the model results for the mixed layer specific humidity and surface temperature (note $T = s/c_p$ at the surface), respectively, for the case of no diabatic heating. No significant drying occurred along any of the streamlines in disagreement with observations which show a minimum in q beneath the anvil. There is a strong gradient of q on the east side of the system; however, observations are very sparse in this region and no meaningful comparison can be made (of course the field variables used in the model are also somewhat uncertain in this part of the squall system). The model predicts rates of surface temperature increases

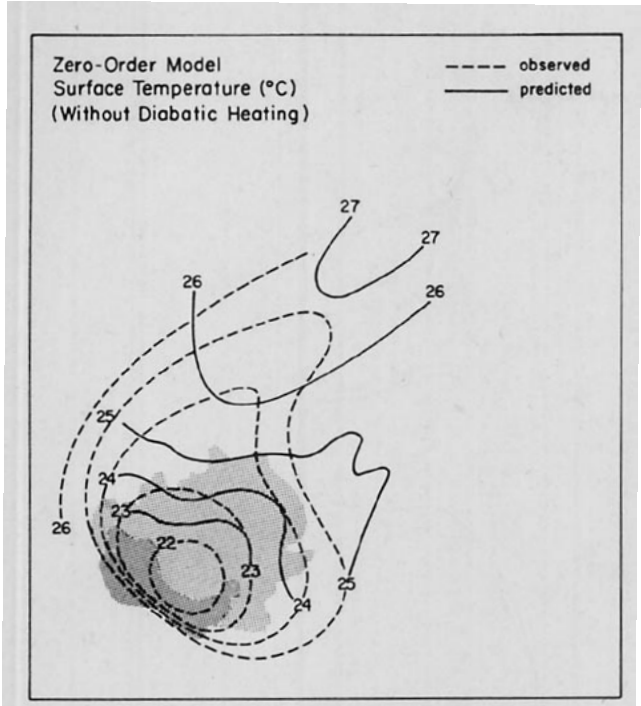

FIG. 12. As in Fig. 11 but for surface temperature (°C).

significantly higher than observations indicate on the north side of the wake, a region where there is fairly good sounding data coverage. The results of the GSEM were found to be very similar to those of the zero-order model.

b. With precipitation evaporation and diabatic heating

The moisture source and associated diabatic heating terms are E_m, ΔE, ΔF_E, LE_m, $L\Delta E$ and $L\Delta F_E$. In determining the mixed-layer evaporation rate E_m, the average temperature between the surface and the mixed layer top was used. A transition layer depth of 80 meters was assumed and the average temperature and specific humidity in this layer was used to estimate ΔF_E. Here ΔE was determined using the temperature and specific humidity at the top and the bottom of the transition layer. For a rainfall rate of 3 mm h^{-1}, a temperature of 22°C and a specific humidity of 15 g kg^{-1}, Eq. (20) gives $E_m \approx 3.5 \times 10^{-8}$ kg m^{-3} s^{-1}, or a heating rate of -0.0875 W m^{-3}. Diabatic heating due to radiation also contributes to the terms involving ΔF_Q, ΔQ and Q_m. Since determination of the radiative fluxes is complicated by the presence of the squall anvil and the magnitude of the heating rate is probably much smaller than that due to precipitation evaporation (-0.023 W m^{-3} if the heating rate were -2°C/day) we neglect this contribution.

Results obtained using the GSEM when precipitation evaporation is included are shown in Fig. 13 for streamline 5 (the model is initiated at the cross along streamline 5 shown in Fig. 9). It is evident that precipitation evaporation can have a significant effect on mixed layer height, dry static energy and specific humidity. Although the results are in only slightly better agreement with observations, they strongly suggest that precipitation evaporation is important. In this particular instance the terms $L\Delta E$ and LE_m are largely responsible for the differences. The effect of evaporation is to make the mixed layer grow more rapidly, substantially reduce the rate of increase of dry static energy, and, unexpectedly, to enhance drying. The evaporation rate is much greater at the top of the transition layer than it is in the mixed layer due to the large jump in Δq. The stronger cooling that occurs at the top of the transition layer tends to reduce Δs_v (since the magnitude of $L\Delta E$ or ΔQ is large in Eq. A2) which increases the entrainment rate and enhances mixed layer drying. This entrainment of dry air has a greater effect on q_m than the direct moistening of the mixed layer by rainfall evaporation. The term LE_m or Q_m in Eq. (A5) plays a major role in reducing the rate of increase of dry static energy.

The observed mixed layer specific humidity reaches a minimum before that predicted by the model. This discrepancy may be because the observed field of specific humidity is a composite in the region of streamline 5 based largely on the data from *Dallas* and *Researcher*. Boom data from *Researcher* are in almost the same region as *Dallas* but some hours later (Fig. 1). Specific humidity observed by *Researcher* reaches a minimum and then increases well before it does at *Dallas*. This difference could be because the observations of specific humidity by *Researcher*, occur between 1800–2000 GMT in this region and the squall line by this time may no longer be in the steady state. On the other hand, composite fields used in the simulation do not use data from *Researcher* at such late times (except that some emphasis is placed on the R(1902) sounding in estimating the gradients of specific humidity and dry static energy above the transition layer).

Also shown in Fig. 13 are the entrainment rate W_{en}, the ratio of the moisture flux at the top of the mixed layer (h) to that at the surface R, and the jumps in dry static energy and specific humidity, Δs and Δq respectively. The entrainment rate is large at the beginning of the integration and decreases to small values at the rear of the squall wake. The ratio R increases to values greater than one which is coincident with drying in the mixed layer (as also noted by Fitzjarrald and Garstang, 1981b). Values of Δq and Δs are in good agreement with observations; Δq increases to values greater than -4 g kg^{-1} and Δs to about 1.8 J g^{-1} which compare favorably to the Q(1823) sounding (see Fig. 5) in the same region.

The results of the GSEM for the fields of specific humidity and surface temperature when rainfall evap-

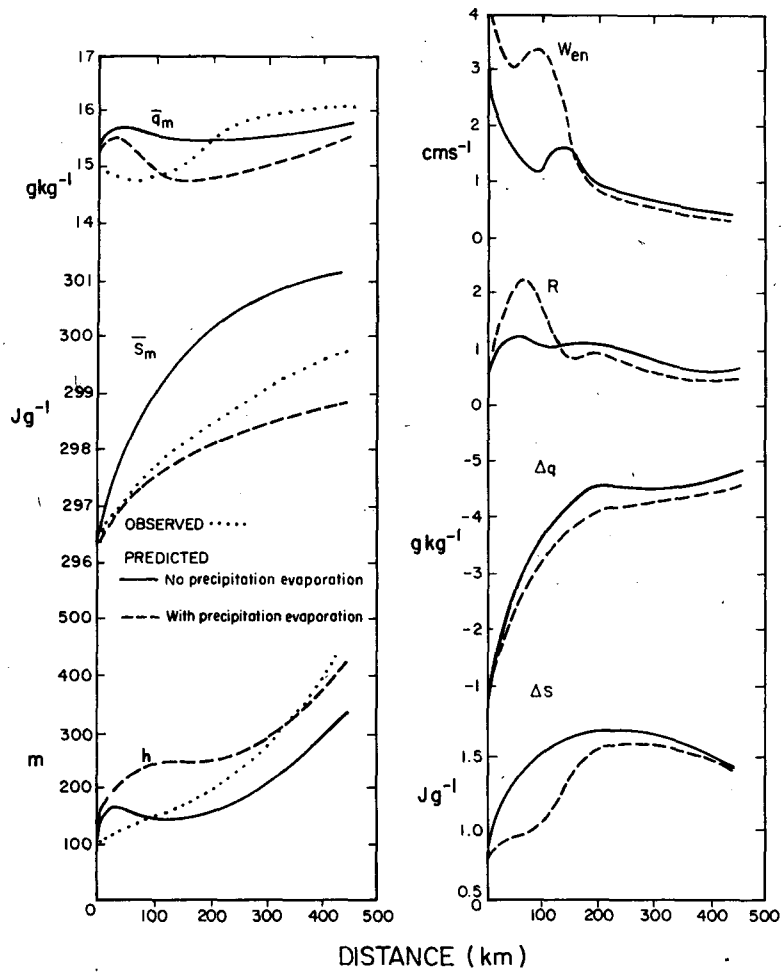

FIG. 13. GSEM values for $\bar{q}_m$, $\bar{s}_m$, h, W_{en}, R, Δq and Δs. Dotted lines are observed values. Results without precipitation evaporation and diabatic heating are solid lines. Dashed lines show results with precipitation evaporation.

oration and diabatic heating are included are shown in Figs. 14 and 15, respectively. Figure 14 is similar to Fig. 11 except that beneath the squall anvil more of a pronounced minimum in mixed-layer specific humidity is obtained in better agreement with observations. Comparison between Fig. 15 and Fig. 12 shows that evaporation in the mixed layer is apparently important for sustaining the cool region in the wake of the squall line, however, now the predicted temperature increases are less than observed.

c. *Sensitivity tests*

In Fig. 16 the sensitivity of h, $\bar{q}_m$ and $\bar{s}_m$ to variations in $\bar{w}_h$, F_{sv}, Γ_s, Γ_q, and v_r using the zero-order model is illustrated. For simplicity moisture source and diabatic heating terms are neglected. Since we are not considering any feedback between the predicted temperatures and specific humidities on the surface fluxes, the model response to a change in specified field variables should only be regarded as an approximation to what would happen in the real atmosphere. (For the changes in specified field variables considered here this feedback is actually fairly small).

Figure 16a shows the results obtained along streamline 5 for the case where $\bar{w}_h = 0.0$ and $\bar{w}_h = -0.02$ m s^{-1} which are held constant, all other variables remaining unaltered. The growth rates of h are quite different than for the case when the observed field of $\bar{w}_h$ is used. When $\bar{w}_h = 0.0$, h grows rapidly, causing the surface temperature increase to be much reduced and larger specific humidities are obtained (note that the rapid growth of h does not imply the entrainment velocity has been increased since $\bar{w}_h$ is now zero). When $\bar{w}_h = -0.02$ m s^{-1} the final mixed layer depth is very low. The resulting mixed-layer dry static energy is larger whereas the specific humidity is less.

Figure 16b shows the results obtained for constant surface buoyancy fluxes of 15 and 30 W m^{-2}. When the buoyancy flux is 30 W m^{-2} quite a rapid growth of h occurs. Strong mixed layer drying is predicted

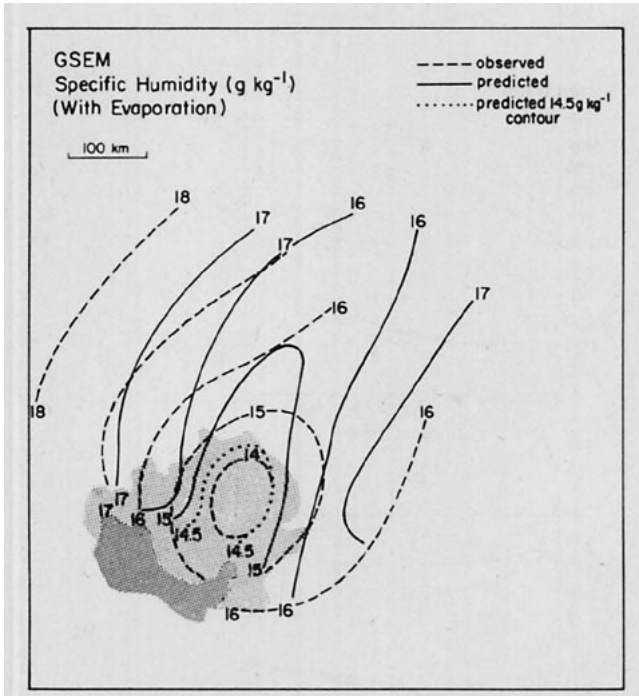

FIG. 14. Mixed layer specific humidity (g kg^{-1}) predicted by the GSEM with evaporation (solid lines). Dashed lines show observed values.

which is due to a large entrainment rate at the top of the mixed layer. Conversely for the case when the buoyancy flux is held at 15 W m^{-2}, mixed layer growth is slower and the entrainment rate is less leading to higher values of specific humidity. Dry static energy increase is substantially reduced when the buoyancy flux is small. Changing the moisture flux F_{q0} (not shown) only has an effect on the mixed layer specific humidity (it does contribute significantly to the buoyancy flux but this can be held constant).

Figure 16c shows the sensitivity to variations in Γ_s. For the case when Γ_s is held constant at 6 J kg^{-1} m^{-1} (which is about the value in front of the squall line) rapid growth of the mixed layer and strong drying occurs. Dry static energy increase is not as fast as when the observed gradients are used since the mixed layer depth is larger. When Γ_s is held at 14 J kg^{-1} m^{-1} the greater stability leads to lower mixed layer heights and thus higher temperatures.

Variations of the gradient of specific humidity have a small effect on the mixed layer depth as can be seen in Fig. 16d where Γ_q is held at -3 g kg^{-1} km^{-1} and -12 g kg^{-1} km^{-1}. Corresponding to these small changes in h only slight differences in dry static energy are observed. However, the predicted mixed layer specific humidity is very sensitive to changes in the lapse rate Γ_q.

We have included advective effects in the equations by integrating along streamlines and using the observed wind speeds. To see the effect of neglecting advection terms we take v_r to be 13.5 m s^{-1} (the speed of the squall line). The results along streamline 5 are shown in Fig. 16e. Streamline 5 runs very nearly parallel to the direction of motion of the squall line, whereas for some streamlines this is not such a good approximation. Figure 16e shows that advection has very little effect on the mixed layer height; however, it does have a noticeable effect on the specific humidity and dry static energy. Neglecting advection changes specific humidity by about 0.4 g kg^{-1} and dry static energy by as much as 0.8 J g^{-1}.

When feedback of predicted temperatures and specific humidities on surface fluxes are considered in a fully interactive model (where the approximation of constant sea surface temperature is made) the results of the sensitivity tests remain qualitatively the same (not shown). Tests were also carried out to find the sensitivity to the initial conditions and the entrainment parameter k. The sensitivity to reasonable variations in h, Δs_v and Δq was small. However, some care was required not to choose Δq initial too large (producing a large F_{qh}) since this would cause drying even for positive values of the gradient of specific humidity above the transition layer. The behavior of Δq following an initially large value is characterized by an initial rapid decrease to a minimum in about 100 km and then a slow increase. The effect of changing the initial value of $\bar{s}_m$ or $\bar{q}_m$ is to shift the predicted curves for these quantities without changing their shape. Varying the entrainment parameter k between 0.2 and 0.4 was also found to make only a small difference to the results.

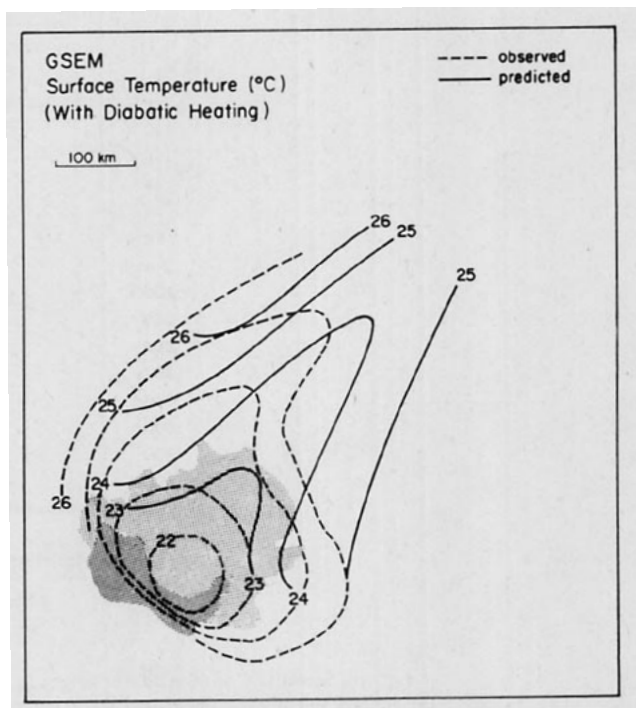

FIG. 15. As in Fig. 14 but for surface temperature (°C).

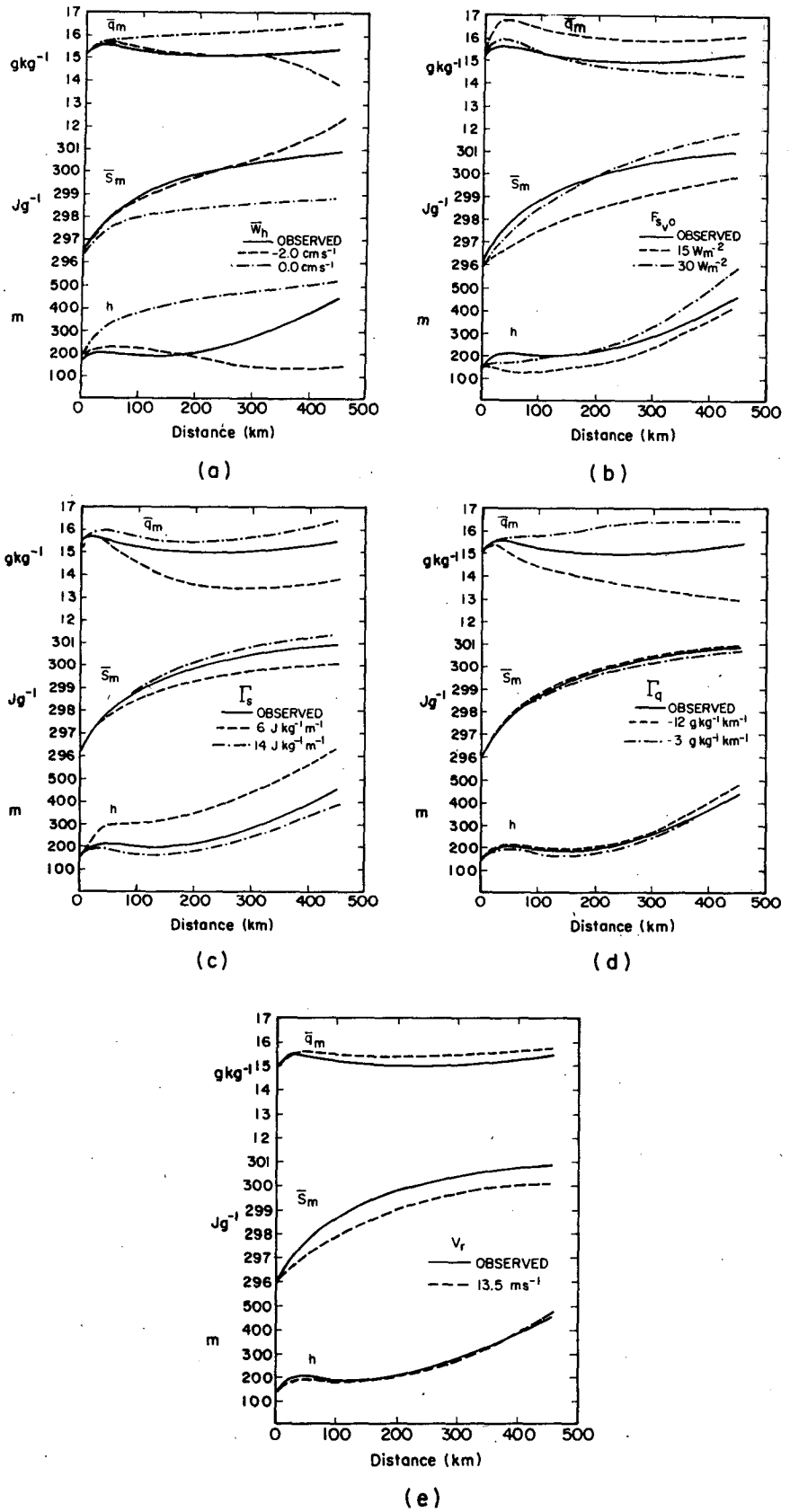

FIG. 16. Sensitivity of mixed layer height h, dry static energy $\bar{s}_m$ and specific humidity $\bar{q}_m$ to: (a) vertical velocity $\bar{\omega}_h$, (b) virtual static energy flux $F_{s_{vo}}$, (c) gradient of dry static energy Γ_s, (d) gradient of specific humidity Γ_q, and (e) inclusion of advective terms.

The importance of knowing with some accuracy the fields of vertical velocity, horizontal velocity, surface fluxes and lapse rates is clearly demonstrated by these sensitivity tests. Reasonable estimates of the errors in the field variables at any point are $\bar{w}$ (± 0.01 m s^{-1} at 375 m), v_r (± 1 m s^{-1}), F_{sv} (± 5 W m^{-2}), Γ_s (± 2 J kg^{-1} m^{-1}), Γ_q (± 3 km^{-1}), although we would not expect systematic errors of this magnitude. Even though errors may be cumulative, we would not expect large disagreements with observations of mixed layer depth and dry static energy due to these field variables (at least based on these error estimates). Model results for mixed-layer specific humidity are very sensitive to lapse rates of specific humidity which has turned out to be a difficult observational quantity to accurately determine.

The strong mesoscale downdraft in the squall wake obviously plays a major role in inhibiting mixed layer growth as found by Fitzjarrald and Garstang (1981b). We also see that the large stability of the air above the transition layer is significant in this regard. Fitzjarrald and Garstang apparently used an average stability between h and 850 mb which could be a significant underestimate since in some soundings the gradient of dry static energy decreases with height above the mixed layer (Fig. 5).

d. Development of thermodynamic profiles

As described in Section 2b, the specific humidity profile has an unusual structure which is apparently caused by advection of air with low specific humidity (originating from convective downdrafts) beneath moister air. Equations (3) and (4), which were used as a qualitative guide to interpreting the development of the thermodynamic profiles, are restrictive because they neglect sources of moisture, diabatic heating and require the lapse rates to be constant. This latter requirement can only be fulfilled if the vertical velocity is a linear function of height. We can fairly easily remove the restriction of constant lapse rate as long as the horizontal velocity is independent of height. Then, as we follow the motion of an air column the change in the lapse rate of specific humidity say, will be due to vertical advection of moisture. The vertical displacement of a parcel along a streamline can be determined from

$$v_r(l)\frac{dz}{dl} = w(l, z). \tag{32}$$

Now if v_r is not a function of height, then $w(l, z)$ will be linear with height (making the incompressible approximation) unless there is a change in the confluence or diffluence of the streamlines in the vertical. If for simplicity we linearly extrapolate from 375 m to obtain the vertical velocity and forward difference Eq. (32) we obtain the results shown in Fig. 17, where

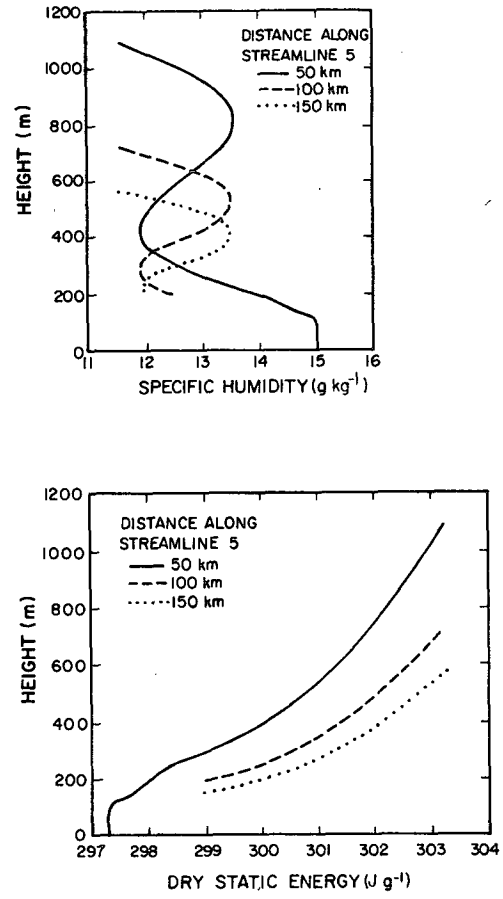

FIG. 17. The effect of subsidence (linear with height) on profiles of specific humidity and dry static energy. Results are shown for integrations along streamline 5. The initial profiles (solid lines) are 50 km along streamline 5; the dashed lines show results at 100 km; the dotted lines at 150 km.

the initial profile was based on the *Researcher* (1902) sounding. The integration was started 50 km along streamline 5 to approximately correspond to the position of the *Researcher* (1902) sounding and the surface relative wind speed was used for $v_r(l)$. The relative maximum in specific humidity approaches the surface faster than observations indicate. At 150 km the predicted relative maxima is at 400 m whereas for the *Quadra* (1823) sounding in this region, shown in Fig. 5, it is at 600 m. This is probably not too surprising in view of the approximation we have made that the vertical velocity is linear with height, likely leading to an overestimate of its magnitude above 375 m.

We can allow w to have a more realistic vertical profile by letting v_r be a function of height. However, to make the problem tractable streamlines have to be considered independent of height; otherwise we would have to trace trajectories from many different regions. This is not very realistic since wind profiles indicate

that there is considerable speed and directional wind shear. This can also be seen in Gamache and Houze (1982, Fig. 6b) for the relative winds at 850 mb which shows the velocity has a large component parallel to the squall line (from the southeast) over much of the anvil region, quite different to the flow at the surface. So, although qualitatively, the effects of subsidence on the thermodynamic profiles can be seen, their development is difficult to determine quantitatively due to the significant speed and directional vertical wind shear.

5. Summary and discussion

In this study a model has been developed for obtaining the two-dimensional fields of mixed layer height, specific humidity and dry static energy in the wake of a GATE tropical squall line. The equations from 1) a zero-order jump mixed-layer model and 2) Deardorff's (1979) general entrainment structure model (GSEM) are formulated relative to the squall system in natural coordinates. The results of the modeling study are in fairly good agreement with observations.

The asymmetry of the mixed layer height found in a composite analysis by Johnson and Nicholls (1983) seems to be well simulated by both models. Mixed layer growth is inhibited by mesoscale subsidence and to a lesser extent (but still significantly) by the large gradient of virtual static energy, above the transition layer. The very stable lapse rate in the wake of the squall is probably mainly due to the mesoscale subsidence, although it could be partly produced within the convective downdraft region. The rapid mixed layer growth on the south east side of the wake can be attributed to the stronger buoyancy flux and weaker subsidence.

The downdraft air within the convective cores that reaches the surface is drier (in an absolute sense) than the air preceding the squall line. It is hypothesized that this dry air advects beneath moister air leading to the unusual specific humidity profiles observed in most of the squall wake soundings. The depth of the convective downdraft outflow is about 1 km at 100 km behind the squall front, within which the gradient of specific humidity above the transition layer is negative. As the mixed layer starts to grow, it entrains drier air from above, which can lead to further reduction of the specific humidity. The mesoscale subsidence leads to a decrease in the depth of the convective downdraft outflow layer so that in some regions the mixed layer depth exceeds it and starts to grow into the air above, which has a relative maxima of specific humidity.

Fitzjarrald and Garstang (1981b) hypothesized that mixed layer drying was a result of rapid mixed layer growth as well as of subsidence as proposed by Zipser (1977). Both of these factors can lead to a large entrainment rates. Obviously the rate of drying will also depend on the difference in moisture content of the entrained air and that of the mixed layer which is very sensitive to the gradient of specific humidity above the transition layer. The largest drying in the squall wake seems to occur in regions of strongly negative gradients of specific humidity which tend to be coincident with strong subsidence. However, it should be emphasized that the composite analysis of the gradients of specific humidity above the transition layer, particularly in the region where they are apparently very large, is based on fairly sparse sounding data, and so the importance of large negative gradients of specific humidity, while suggestive, cannot yet be regarded as conclusive. The results of this study suggest that rainfall evaporation can also contribute significantly to drying by increasing the mixed layer growth rate. The situation is further complicated by the fact that mixed-layer specific humidity also depends on the surface moisture flux. Hence, these results for the mixed-layer specific humidity prediction differ from those of Fitzjarrald and Garstang (1981b), since we find that large negative gradients of specific humidity above the transition layer and rainfall evaporation appear essential to explaining the observed mixed layer drying that occurred in the wake of this squall line.

Model results suggest rainfall evaporation plays an important role in sustaining the cool region within the squall wake. In a fully interactive model where surface fluxes are predicted, say, using bulk aerodynamic expressions, rather than taken as observed, then mixed layer cooling due to rainfall evaporation might, in principle, modify the predictions of the mixed layer depth. For instance, if precipitation evaporation were neglected in a fully interactive model then the predicted mixed layer temperature would be higher leading to reduced surface fluxes and hence shallower predicted mixed layer depths. Fortunately, however, for the realistic rainfall evaporation estimates used here, the predicted and observed surface fluxes have been found to be in relatively good agreement, thus justifying and making internally consistent the approach adopted in this study.

Although a number of approximations have been made in this modeling study it represents a considerable improvement over previous works of this kind. Among the improvements are: modeling of the two dimensional mixed layer height and thermodynamic fields, inclusion of the time varying fields of all the externally specified parameters, advective terms, the effects of diabatic heating and a finite transition layer depth. The zero-order model seems to work reasonably well giving results that differ little from those of the GSEM which has a finite transition layer depth.

Acknowledgments. The authors thank Drs. Duane Stevens and Wayne Schubert for valuable comments and discussion. The careful review of Dr. Gary Barnes has been quite helpful. We have also benefited from discussion with Mr. Francis Crum and Mr. Gregory Tripoli. Mr. Tripoli provided the algorithm we have used to compute precipitation evaporation. Special thanks are extended to Ms. Machel Sandfort for typing the manuscript.

This research has been supported by the Division of Atmospheric Sciences, National Science Foundation under Grants ATM-8015347 and ATM-8206808.

APPENDIX

GSEM Equations

The predictive equations for the GSEM were derived by Deardorff (1979). With the inclusion of diabatic terms the equations become

$$w_{e1} = \frac{1}{\Delta s_v(1 - GY)}\left[\alpha(1 - Y)F_{sv0} - \Delta s_v(1 - Y - GY)\left(\frac{d\Delta h}{dt} - \Delta w\right) - \alpha\frac{(F_{Qh_1} - F_{Q0})}{\rho} + \frac{(F_{Qh_2} - F_{Qh_1})}{\rho} + Y\Delta h\Delta Q\right], \quad \text{(A1)}$$

$$\frac{d\Delta s_v}{dt} = \Gamma_{s_v}\left(w_{e1} + \frac{d\Delta h}{dt} - \Delta w\right) + \frac{F_{s_vh_1} - F_{sv0}}{h_1} + \Delta Q, \quad \text{(A2)}$$

$$F_{qh_1} = \frac{1}{(1 + \alpha - \alpha Y)}\left[-w_{e1}(1 - G_qY)\Delta q + \alpha(1 - Y)F_{q0} - (1 - Y - G_qY)\Delta q\left(\frac{d\Delta h}{dt} - \Delta w\right) - \alpha\frac{(F_{Eh_1} - F_{E0})}{\rho} + \frac{(F_{Eh_2} - F_{Eh_1})}{\rho} + Y\Delta h\Delta E\right], \quad \text{(A3)}$$

$$\frac{d\Delta q}{dt} = \Gamma_q\left(w_{e1} + \frac{d\Delta h}{dt} - \Delta w\right) + \frac{F_{qh_1} - F_{q0}}{h_1} + \Delta E, \quad \text{(A4)}$$

$$\frac{d\bar{s}_{vm}}{dt} = \frac{F_{sv0}}{h_1} + Q_m, \quad \text{(A5)}$$

$$\frac{d\bar{q}_m}{dt} = \frac{F_{q0} - F_{qh_1}}{h_1} + E_m, \quad \text{(A6)}$$

where

- h_1 mixed layer height
- h_2 height to the top of the transition layer
- Δh transition layer depth (held constant in this study).
- Δw difference in vertical velocity between the top and bottom of the transition layer
- Y integral shape factor (see Deardorff, 1979)
- α $\Delta h/h_1$
- w_{e1} $dh_1/dt - w_{h_1}$
- G $\Gamma_{S_v}\Delta h/\Delta S_v$
- G_q $\Gamma_q\Delta h/\Delta q$.

Other terms are as defined in the zero-order model.

REFERENCES

Arakawa, A., and W. H. Schubert, 1974: Interaction of a cumulus cloud ensemble with the large-scale environment. Part I: *J. Atmos. Sci.*, **31**, 674–701.

Aspliden, C. I., Y. Tourre and J. B. Sabine, 1976: Some climatological aspects of West African disturbance lines during GATE. *Mon. Wea. Rev.*, **104**, 1029–1035.

Ball, F. K., 1960: Control of inversion height by surface heating. *Quart. J. Roy. Meteor. Soc.*, **86**, 483–494.

Barnes, G. M., and M. Garstang, 1982: Subcloud layer energetics of precipitating convection. *Mon. Wea. Rev.*, **110**, 102–117.

Betts, A. K., 1973: Non-precipitating cumulus convection and its parameterization. *Quart. J. Roy. Meteor. Soc.*, **99**, 178–196.

——, 1976: The thermodynamic transformation of the tropical subcloud layer by precipitation and downdrafts. *J. Atmos. Sci.*, **33**, 1008–1020.

Carson, D. J., 1973: The development of a dry inversion-capped convectively unstable boundary layer. *Quart. J. Roy. Meteor. Soc.*, **99**, 450–467.

Cox, S. K., and K. T. Griffith, 1979: Estimates of radiative divergence during Phase III of the GARP Atlantic Tropical Experiment. Part II: Analysis of Phase III results. *J. Atmos. Sci.*, **36**, 586–601.

Deardorff, J. W., 1979: Prediction of convective mixed-layer entrainment for realistic capping inversion structure. *J. Atmos. Sci.*, **36**, 424–436.

Driedonks, A. J. M., 1982: Models and observations of the growth of the atmospheric boundary layer. *Bound.-Layer Meteor.*, **23**, 283–306.

Fitzjarrald, D. R., and M. Garstang, 1981a: Vertical structure of the tropical boundary layer. *Mon. Wea. Rev.*, **109**, 1512–1526.

——, and ——, 1981b: Boundary layer growth over the tropical ocean. *Mon. Wea. Rev.*, **109**, 1762–1772.

Gamache, J. F., and R. A. Houze, Jr., 1982: Mesoscale air motions associated with a tropical squall line. *Mon. Wea. Rev.*, **110**, 118–135.

——, and ——, 1983: Water budget of a mesoscale convective system in the tropics. *J. Atmos. Sci.*, **40**, 1835–1850.

Gaynor, J. E., and P. A. Mandics, 1978: Analysis of the tropical marine boundary layer during GATE using acoustic sounder data. *Mon. Wea. Rev.*, **106**, 223–232.

——, and C. F. Ropelewski, 1979: Analysis of the convectively modified GATE boundary layer using *in situ* and acoustic sounder data. *Mon. Wea. Rev.*, **107**, 985–993.

Holle, R. L., S. W. Leavitt, J. Simpson, R. Biondini and J. W. Snow, 1977: Cloudiness from whole-sky pictures taken aboard four U.S. B-scale ships. Dept. Environ. Sci., University of Virginia, 293 pp. [Microfilm from World Data Center—A (GATE), Asheville, NC]

Houze, R. A., Jr., 1977: Structure and dynamics of a tropical squall-line system observed during GATE. *Mon. Wea. Rev.*, **105**, 1540–1567.

Johnson, R. H., 1981: Large-scale effects of deep convection on the GATE tropical boundary layer. *J. Atmos. Sci.*, **38**, 2399–2413.

——, and M. E. Nicholls, 1983: A composite analysis of the boundary layer accompanying a tropical squall line. *Mon. Wea. Rev.*, **111**, 308–319.

Leary, C. A., and R. A. Houze, Jr., 1979: Melting and evaporation of hydrometeors in precipitation from the anvil clouds of deep tropical convection. *J. Atmos. Sci.*, **36**, 669–679.

Lilly, D. K., 1968: Models of cloud-topped mixed layers under a strong inversion. *Quart. J. Roy. Meteor. Soc.*, **94**, 292–309.

Moore, M. J., and R. R. Long, 1971: An experimental investigation of turbulent stratified shearing flow. *J. Fluid Mech.*, **49**, 635–655.

Payne, S. W., and M. M. McGarry, 1977: The relationship of satellite inferred convective activity to easterly waves over West Africa and the adjacent ocean during Phase III of GATE. *Mon. Wea. Rev.*, **105**, 413–420.

Schubert, W. H., J. S. Wakefield, E. J. Steiner and S. K. Cox, 1979a: Marine stratocumulus convection. Part I: Governing equations and horizontally homogeneous solutions. *J. Atmos. Sci.*, **36**, 1286–1307.

——, ——, —— and ——, 1979b: Marine stratocumulus convection. Part II: Horizontally inhomogeneous solutions. *J. Atmos. Sci.*, **36**, 1308–1324.

Tennekes, H., 1973: A model for the dynamics of the inversion above a convective layer. *J. Atmos. Sci.*, **30**, 558–567.

Tripoli, G. J., and W. R. Cotton, 1980: A numerical investigation of several factors contributing to the observed variable intensity of deep convection over south Florida. *J. Appl. Meteor.*, **19**, 1037–1063.

Willis, P. T., 1984: Functional fits to some observed drop size distributions and parameterization of rain. *J. Atmos. Sci.*, **41**, 1648–1661.

Zipser, E. J., 1977: Mesoscale and convective-scale downdrafts as distinct components of squall-line structure. *Mon. Wea. Rev.*, **105**, 1568–1589.